Contents lists available at ScienceDirect

Solar Energy Materials & Solar Cells

Dielectric function and double absorption onset of monoclinic Cu$_2$SnS$_3$: Origin of experimental features explained by first-principles calculations

Andrea Crovetto [a,*], Rongzhen Chen [b], Rebecca Bolt Ettlinger [c], Andrea Carlo Cazzaniga [c], Jørgen Schou [c], Clas Persson [b,d], Ole Hansen [a,e,*]

[a] DTU Nanotech, Technical University of Denmark, DK-2800 Kgs. Lyngby, Denmark
[b] Department of Materials Science and Engineering, Royal Institute of Technology, SE-100 44 Stockholm, Sweden
[c] DTU Fotonik, Technical University of Denmark, DK-4000 Roskilde, Denmark
[d] Department of Physics, University of Oslo, PO Box 1048 Blindern, NO-0316 Oslo, Norway
[e] CINF, Center for Individual Nanoparticle Functionality, Technical University of Denmark, Technical University of Denmark, DK-2800 Kgs. Lyngby, Denmark

ARTICLE INFO

ABSTRACT

In this work, we determine experimentally the dielectric function of monoclinic Cu$_2$SnS$_3$ (CTS) by spectroscopic ellipsometry from 0.7 to 5.9 eV. An experimental approach is proposed to overcome the challenges of extracting the dielectric function of Cu$_2$SnS$_3$ when grown on a glass/Mo substrate, as relevant for photovoltaic applications. The ellipsometry measurement reveals a double absorption onset at 0.91 eV and 0.99 eV. Importantly, we demonstrate that calculation within the density functional theory (DFT) confirms this double onset only when a very dense **k**-mesh is used to reveal fine details in the electronic structure, and this can explain why it has not been reported in earlier calculated spectra. We can now show that the double onset originates from optical transitions at the Γ-point from three energetically close-lying valence bands to a single conduction band. Thus, structural imperfection, like secondary phases, is not needed to explain such an absorption spectrum. Finally, we show that the absorption coefficient of CTS is particularly large in the near-band gap spectral region when compared to similar photovoltaic materials.

© 2016 Elsevier B.V. All rights reserved.

1. Introduction

The ternary chalcogenide semiconductor Cu$_2$SnS$_3$ (CTS) has attracted interest as a solar cell absorber material in the last half decade. Indeed, promising power conversion efficiencies of 4.63% and 4.29% have recently been reported by two independent groups [1,2]. The main potential advantage of CTS over quaternary absorbers Cu(In, Ga)Se$_2$ (CIGS), Cu$_2$ZnSnS$_4$ (CZTS), and Cu$_2$ZnSnSe$_4$ (CZTSe) is a relatively broad single-phase region and reduced fabrication complexity due to fewer chemical constituents [3]. Furthermore, the CTS compound consists of inexpensive and non-toxic chemical elements, unlike the common high-efficiency chalcogenide absorbers CIGS and CdTe. CTS is typically produced by high temperature sulfurization of metal precursors [1] or of a precursor S-containing compound [2,3].

Depending on the deposition parameters and sulfurization conditions, CTS can form with different crystal structures. Tetragonal, cubic, monoclinic, and triclinic phases have been reported. Despite such phase variety, a theoretical work [4] has shown that all the commonly observed crystal structures are based on the same zincblende pattern with tetrahedral coordination. The only difference between them is the degree of disorder in the cation sublattice, which results in different crystal symmetries. The monoclinic phase is a perfectly ordered phase, whereas the disordered cubic and tetragonal phases feature different arrangements of tetrahedral S-Cu$_2$Sn$_2$ and S-Cu$_3$Sn structural motifs. The best-performing CTS solar cells reported so far had a CTS absorber with monoclinic structure [1,2].

A double absorption onset of 0.90–0.93 eV and 0.97–1.02 eV [1,5,6] has consistently been reported in the literature for monoclinic CTS, on the basis of both optical absorption and quantum efficiency (QE) measurements. It has been shown [7] that the double onset is an intrinsic feature of monoclinic CTS and it does not arise from other CTS phases or other compounds. However, another study [8] has shown that a disordered structure can exist

* Correspondence to: Ørsteds Plads, building 345 East, DK-2800 Kgs. Lyngby, Denmark
E-mail addresses: ancro@nanotech.dtu.dk (A. Crovetto), ole.hansen@nanotech.dtu.dk (O. Hansen).

locally even in single-phase monoclinic CTS due to the high density of structural defects such as stacking faults, which modify the local atomic coordination. This leaves the open question of whether the double onset is a feature of defect-free monoclinic CTS, or if it is a consequence of the high defect density found in CTS thin films, which locally alters its band structure and consequently its optical transitions. While the electronic structure and density-of-states of monoclinic CTS have earlier been analyzed theoretically [4,9–11] and the optical properties have been computed [4,9], the double onset phenomenon was not reported in those studies. Furthermore, no experimental data on the dielectric function of monoclinic CTS is found in the literature. Experimental dielectric functions have only been reported for multi-phase films identified as a mix of tetragonal and cubic CTS [12], where it is not possible to isolate the dielectric functions of the two single phases.

In this work, we synthesize thin films of monoclinic CTS by pulsed laser deposition (PLD) on Mo-coated glass in order to reproduce the conditions under which CTS is formed in solar cell devices. We extract the complex dielectric function $\varepsilon(E) = \varepsilon_1(E) + i\varepsilon_2(E)$ of CTS in the photon energy range from $E = 0.7$–5.9 eV by spectroscopic ellipsometry measurement, and compare it to the dielectric function calculated within the density functional theory (DFT) to corroborate the results and to investigate the origin of the double onset phenomenon. We find that the very details in the dielectric response at the band-gap energy are revealed only with a very dense **k**-point sampling. Then, the double onset phenomenon is explained as optical transitions from the three topmost bands at the valence band maximum (VBM) in a perfectly crystalline CTS. Thus, the phenomenon does not need to be due to structural imperfections, like a disordered structure or secondary phases. Also, with the dense **k**-mesh the shapes of both the real and imaginary parts of the dielectric function are improved considerably in the low energy region (i.e., below 1.5 eV).

2. Experimental details

Thin films of Mo (approximately 500 nm thick) were deposited on soda lime glass (SLG) by DC magnetron sputtering, with a sputtering pressure of 1.3×10^{-2} mbar for the first 200 nm (adhesion layer) and 3.9×10^{-3} mbar for the last 300 nm (low-resistivity layer).

Thin films of Cu_2SnS_3 were deposited at room temperature on Mo-coated soda lime glass substrates in a pulsed laser deposition (PLD) setup with a background pressure below 3×10^{-6} mbar. The substrates were cleaned sequentially by ultrasonic treatment for 5 min in acetone and isopropanol and finally rinsed in ultrapure water. The laser beam from a Nd: YAG laser (355 nm wavelength, 7 ns pulse duration) with a repetition rate of 10 Hz was partly focused onto a beam-spot of 2.2 mm^2 with an angle of incidence of 45° with respect to the target normal and a target-substrate distance of 4.4 cm, as illustrated in Fig. 1. The laser fluence was set to 1.6 J/cm^2. The targets used are sintered powder disks provided by Testbourne Ltd. with the stoichiometry Cu_2SnS_3.

After deposition, the samples were annealed at 570 °C for 10 min in a sealed furnace evacuated down to 10^{-4} mbar and then filled with 100 mbar of N_2 gas. Samples were placed in a graphite box in the hot zone of the furnace together with 160 mg of sulfur.

The films were imaged with a scanning electron microscope (SEM) equipped with a field emission gun (FE-SEM, Supra 60 VP, Zeiss). Energy dispersive X-ray spectroscopy (EDX) was performed in the same instrument using a silicon drift detector (X-Max^N 50, Oxford Instruments) and a beam voltage of 15 kV. EDX spectra were taken on five different spots and averaged. The error bars are expressed as the standard deviation of the measurements. The EDX analysis software (AzTec, Oxford Instruments) was calibrated with elemental standards instead of with a reference compound.
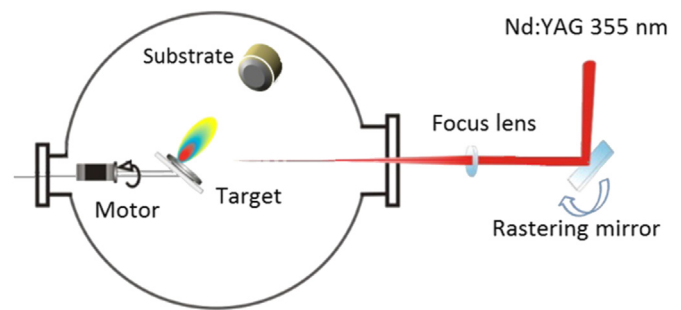

Fig. 1. Scheme of the pulsed laser deposition setup. The combination of target rotation and a rastering mirror ensures uniform ablation of the target. In a vacuum chamber a pulsed laser source (Nd: YAG, 355 nm, 7 ns pulses at 10 Hz) is focused onto a target, which is ablated by the laser.

Therefore, we expect the standard error due to an oversimplified EDX spectrum analysis to be larger than the standard deviation of the measurements.

X-ray diffraction (XRD) patterns were collected with a Bruker D8 powder diffractometer in Bragg-Brentano configuration using $Cu - K_\alpha$ radiation, a 0.009° step size, and a 1.5 s/step integration time. In order to avoid possible peak shifts due to sample alignment errors, the diffraction pattern was aligned using the peaks of standard Si powder.

Raman spectra were obtained in the backscattering configuration at a laser wavelength of 455 nm and laser power of 1.6 mW, using a 50 × objective that resulted in a spot size of about 2 μm × 2 μm (DXR Raman Microscope, Thermo Scientific).

Ellipsometry measurements were performed in reflection mode in the spectral range 0.7–5.9 eV on a rotating compensator spectroscopic ellipsometer (M-2000, J.A. Woollam Co.) using a collimated beam with a spot size of approximately 200 μm × 300 μm. Ellipsometry spectra were analyzed and fitted with the CompleteEase software package (version 5.06- J.A. Woollam Co.). When properties of a thin film are to be extracted by an ellipsometry measurement, the reliability of the results depends strongly on the amount of unknown fitting parameters, versus the number of independent measured variables that can be used to fit such parameters [13]. In order to increase the number of measured variables, we measured the magnitude ($\tan \Psi$) and phase (Δ) of the ratio between p- and s- type polarization reflection coefficients for six angles of incidence (from 45 to 70° in steps of 5°), giving twelve measured variables at each wavelength, which were fitted simultaneously in the data analysis step. In order to decrease the number of fitting parameters, we extracted the dielectric function of each layer independently in a separate ellipsometry measurement, as explained in the following sections. A Kramers–Kronig-consistent b-spline model was used to model the shape of the dielectric functions, as demonstrated previously [14]. This means that the imaginary part $\varepsilon_2(E)$ was fitted by a b-spline function using control points spaced by 0.2 eV, whereas the real part $\varepsilon_1(E)$ was not fitted independently but was instead derived by Kramers–Kronig integration. This implies that the relation between $\varepsilon_1(E)$ and $\varepsilon_2(E)$ is a physical one, and that one fitting parameter, instead of two, is required at each control point. Bruggeman's effective medium theory [13] was employed to treat surface roughness as a 50%-solid-film-50%-air layer. Unless otherwise stated, the thickness of the films and of the surface roughness layer were treated as unknown parameters and fitted in the model. However, in order to constrain their range to realistic values and reduce potential correlation errors, their initial values were assigned on the basis of measurements done with other techniques. Since all the layers of interest for this study can be clearly identified in cross sectional SEM images (Fig. 2), pixel counting from high-resolution SEM images allowed us to estimate film thicknesses. In the case of surface roughness, the